Int. J. Heat Mass Transfer. Vol. 36, No. 9, pp. 2339–2347, 1993
Printed in Great Britain

0017–9310/93 $6.00 + 0.00

Effects of longitudinal vortex generators on heat transfer and flow loss in turbulent channel flows

J. X. ZHU, N. K. MITRA and M. FIEBIG
Institut für Thermo- und Fluiddynamik, Ruhr-Universität Bochum, D-4630 Bochum 1, F.R.G.

(*Received* 30 *March* 1992 *and in final form* 22 *September* 1992)

Abstract—The influences of four types of longitudinal vortex generators (delta wing, rectangular wing, delta winglet pair and rectangular winglet pair) on heat transfer and flow loss in turbulent channel flows are investigated in the present work. A numerical solver of the Navier–Stokes equations, based on the MAC algorithm, has been extended with the k–ε turbulence model for this study. The results show that the longitudinal vortices produced by the vortex generators elevate significantly the level of turbulence kinetic energy in the flows and strongly disturb the thermal boundary layer. The mean heat transfer rate can be increased by 16–19% with the vortex generators for an area of channel wall which is 30 times larger than the vortex generator area. The ratio of heat transfer enhancement and flow loss increase indicates better performance for the rectangular winglet pair.

1. INTRODUCTION

TURBULENT flows and heat transfer in a parallel wall channel occur frequently in many heating and cooling devices. A typical example is a plate fin heat exchanger. Figure 1 shows a configuration of a finned tube heat exchanger, which consists of an array of channels with parallel walls. Generally a liquid flows through the tubes and a gas flows through the channels formed by parallel plate fins. In the channels boundary layers grow along the two opposite channel walls. The growth of the boundary layer increases the thermal resistance between the fluid and the channel walls.

In order to enhance heat transfer at the channel walls, longitudinal vortex generators can be placed at the plates, e.g. refs. [1–4]. The vortex generators, mostly slender wings or winglets at high angle of attack (see Fig. 2), generate strong longitudinal vortices which rotate the flow, substitute fluid from the wall region by fluid with higher momentum from the core region of the channel (e.g. Fig. 3) and thus enable high rates of heat transfer at the plates. Longitudinal vortices have a strong influence on momentum and heat transfer far downstream of their origin even in turbulent flow, e.g. ref. [4]. The ordered vortex motion should result in higher heat transfer at lower flow loss increase than at a purely higher Reynolds number level.

Fiebig *et al.* [2, 3] have investigated the heat transfer enhancement and drag increase produced by a single, slender delta wing, rectangular wing or winglets attached to a channel wall for laminar flows. Eaton and coworkers at Stanford University [4, 5] observed experimentally the interactions of a pair of embedded delta winglets with two-dimensional and three-dimensional turbulent boundary layers and their influence on heat transfer at wall.

The purpose of the present work is to predict effects of different forms of vortex generators such as delta wing, delta winglet pairs, rectangular wing and winglet pairs (Fig. 2) on heat transfer and flow losses in turbulent channel flows.

2. MATHEMATICAL FORMULATION

2.1. *Computational domain*

Figure 4 shows the computational domain consisting of a parallel wall channel and a pair of delta winglets (DWP) which can be replaced by other forms such as a rectangular winglet pair (RWP), delta wing (DW) and rectangular wing (RW), see Fig. 2. Table 1 gives the geometrical parameters of the vortex generators with respect to the channel height H. The surface areas of the vortex generators and their angle of attack ($\beta = 25°$) are kept equal for all cases.

The geometrical parameters of the computational

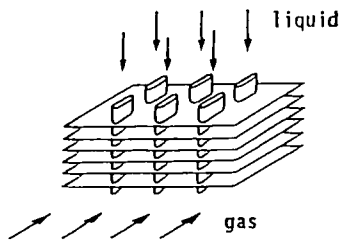

FIG. 1. Schematic of a compact gas–liquid heat exchanger with extended surfaces (finned tube).

NOMENCLATURE

A	Van Driest's constant for the mixing length
A_f	frontal area ($A_f = B \cdot H$) [m^2]
B	channel width [m]
c_1, c_2, c_μ	constants in k–ε model
c_p	specific heat at constant pressure [J kg^{-1} K^{-1}]
C_φ	dissipation number, equation (24)
D_h	hydraulic diameter for the cross section [m]
E	constant in logarithmic law of the wall
f	dependent variables
f_{app}	apparent friction factor
G	production of turbulence kinetic energy [kg m^{-1} s^{-3}]
H	channel height [m]
k	turbulence kinetic energy [m^2 s^{-2}]
L	channel length [m]
M	mass flow rate [kg s^{-1}]
Nu	Nusselt number
p	static pressure [N m^{-2}]
P_D	dissipation, equation (23) [W]
Pr	Prandtl number
Pr_t	turbulent Prandtl number
q_w	wall heat flux per unit area [W m^{-2}]
Re	Reynolds number ($\rho U_o D_h/\mu$)
Re_H	Reynolds number ($\rho U_o H/\mu$)
t	time [s]
T_B	bulk temperature [K]
T_o	entrance temperature [K]
T_w	wall temperature [K]
U	streamwise velocity [m s^{-1}]
U_o	mean velocity [m s^{-1}]
U_i	time-averaged velocity [m s^{-1}]
V	velocity in vertical direction [m s^{-1}]
W	spanwise velocity [m s^{-1}]
x	streamwise coordinate [m]
x_i	Cartesian coordinates [m]
y	vertical coordinate [m]
y^+	wall coordinate
z	spanwise coordinate [m].

Greek symbols

α	heat transfer coefficient [W m^{-2} K^{-1}]; kinetic energy correction factor, equation (22)
β	angle of attack of vortex generator [°]
Γ	thermal diffusivity [kg m^{-1} s^{-1}]
Γ_t	turbulent thermal diffusivity
δ	Kronecker delta
ε	dissipation rate of turbulence energy [m^2 s^{-3}]
κ	von Karman constant
λ	thermal conductivity [W m^{-1} K^{-1}]
μ	molecular viscosity [N s m^{-2}]
μ_t	turbulent viscosity
ρ	density [kg m^{-3}]
σ_k, σ_ε	turbulent 'Prandtl number' for diffusion of k and ε
τ_w	wall shear stress, [N m^{-2}]
Φ_{12}	specific dissipation, equation (22) [m^2 s^{-2}]
ω_x	vorticity [s^{-1}]
$\bar{\omega}_x$	average vorticity, equation (18) [s^{-1}].

Subscripts

m	average value
o	value of the base flow.

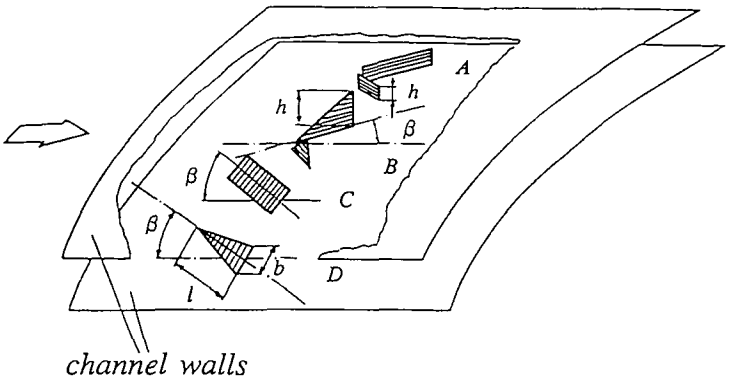

FIG. 2. Some types of longitudinal vortex generators: A) Rectangular Winglet Pair (RWP); B) Delta Winglet Pair (DWP); C) Rectangular Wing (RW); D) Delta Wing (DW).

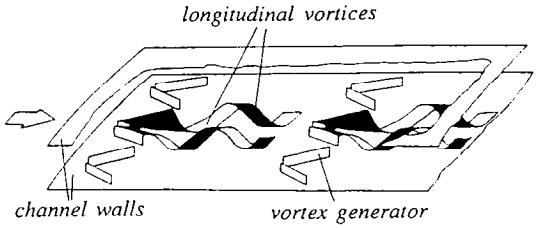

FIG. 3. Schematic of flow separation at the edges of the vortex generators and formation of longitudinal vortices in a channel flow.

domain (Fig. 4) have the following values relative to the channel height H:

$$L = 10H, \quad B = 6H, \quad a = 0.5H.$$

The flows are assumed to be symmetric about the centre plane (II), so that the computations are performed only in the region between the planes I and II in the z-direction.

2.2. *Governing equations*

The three-dimensional Reynolds averaged Navier–Stokes and energy equations in conjunction with the eddy viscosity concept are used to describe the incompressible flows in the computational domain [6]. These equations are written in a Cartesian tensor form as:

Continuity

$$\frac{\partial U_i}{\partial x_i} = 0 \tag{1}$$

Momentum

$$\rho \frac{\mathrm{D}U_i}{\mathrm{D}t} = -\frac{\partial p}{\partial x_i} + \frac{\partial}{\partial x_i}\left[(\mu+\mu_t)\left(\frac{\partial U_i}{\partial x_j} + \frac{\partial U_j}{\partial x_i}\right) - \tfrac{2}{3}\rho k \delta_{ij}\right] \tag{2}$$

Energy

$$\rho \frac{\mathrm{D}T}{\mathrm{D}t} = \frac{\partial}{\partial x_i}\left[(\Gamma+\Gamma_t)\frac{\partial T}{\partial x_i}\right] \tag{3}$$

Table 1. Geometrical parameters of the vortex generators (e.g. Figs. 2 and 4)

	DWP	RWP	DW	RW
l	$2H$	$2H$	$2H$	$2H$
b			$2H$	$1H$
h	$1H$	$0.5H$		
s	$0.5H$	$0.5H$		

where the turbulent viscosity μ_t and the turbulent dynamic thermal diffusivity Γ_t are given by

$$\mu_t = c_\mu \rho k^2/\varepsilon \tag{4}$$

$$\Gamma_t = \frac{\mu_t}{Pr_t}. \tag{5}$$

The turbulence kinetic energy k and its dissipation rate ε are computed from the standard k–ε model of Launder and Spalding [7]:

$$\rho \frac{\mathrm{D}k}{\mathrm{D}t} = \frac{\partial}{\partial x_i}\left(\frac{\mu_t}{\sigma_k}\frac{\partial k}{\partial x_i}\right) + G - \rho\varepsilon \tag{6}$$

$$\rho \frac{\mathrm{D}\varepsilon}{\mathrm{D}t} = \frac{\partial}{\partial x_i}\left(\frac{\mu_t}{\sigma_\varepsilon}\frac{\partial \varepsilon}{\partial x_i}\right) + c_1 \frac{\varepsilon}{k} G - c_2 \rho \frac{\varepsilon^2}{k}. \tag{7}$$

G denotes the production rate of k which is given by:

$$G = \mu_t \left(\frac{\partial U_i}{\partial x_j} + \frac{\partial U_j}{\partial x_i}\right)\frac{\partial U_i}{\partial x_j}. \tag{8}$$

The standard constants [7] are employed:

$$c_\mu = 0.09, \quad c_1 = 1.44, \quad c_2 = 1.92,$$
$$\sigma_k = 1.0, \quad \sigma_\varepsilon = 1.3, \quad Pr_t = 0.9.$$

2.3. *Boundary conditions*

Entrance. Hydrodynamically developed flow and a uniform temperature T_0 are assumed at the inlet of the channel in the present study. The inlet velocity, k

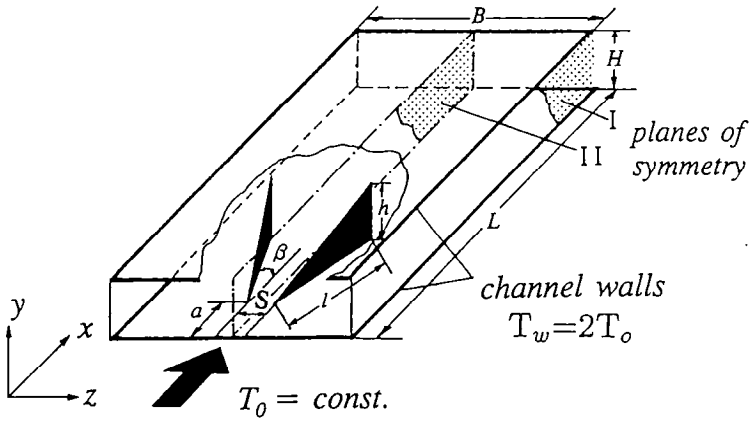

FIG. 4. Computational domain: A parallel wall channel with a delta winglet pair mounted on the channel bottom wall. In a fin-plate heat exchanger the element may be repeated in spanwise and vertical directions.

and ε profiles are obtained from a calculation of two-dimensional turbulent duct flow.

Exit. At the outlet the streamwise gradients of all variables are set to zero:

$$\frac{\partial f}{\partial x} = 0; \quad f = \{U, V, W, k, \varepsilon, T\}. \tag{9}$$

Symmetry. At the symmetry planes (I and II) the normal velocity component and the normal derivatives of all other variables are set to zero:

$$W = 0; \quad \frac{\partial f}{\partial z} = 0; \quad f = \{U, V, k, \varepsilon, T\}. \tag{10}$$

Walls. Wall functions given by Launder and Spalding [7] are employed to prescribe the boundary conditions along the channel walls. The wall functions are applied in terms of diffusive wall fluxes. For the wall-tangential moment these are the wall shear stresses:

$$\tau_w = \frac{\rho U_p c_\mu^{1/4} k_p^{1/2} \kappa}{\ln (E y^+)} \tag{11}$$

with the non-dimensional wall distance y^+ defined as:

$$y^+ = \frac{\rho y_p c_\mu^{1/4} k_p^{1/2}}{\mu} \tag{12}$$

and $\kappa \simeq 0.42$, $E = 9.0$.

The subscript p refers to the grid point adjacent to the wall. The production rate of k and the averaged dissipation rates over the near-wall cell for the k-equation as well as the value of ε at the point p are computed respectively from following equations [7, 8]:

$$G_p = \tau_w \frac{U_p}{y_p} \tag{13}$$

$$\bar{\varepsilon} = \frac{1}{y_p} \int_0^{y_p} \varepsilon \, dy = \frac{c_\mu^{3/4} k_p^{3/2}}{\kappa y_p} \ln (E y^+) \tag{14}$$

$$\varepsilon_p = c_\mu^{3/4} \frac{k_p^{3/2}}{\kappa y_p}. \tag{15}$$

For the temperature boundary condition, the heat flux to the wall is derived from the thermal wall function [7]:

$$q_w = \frac{(T_w - T_p) \rho c_p c_\mu^{1/4} k_p^{1/2}}{Pr_t \left[\frac{1}{\kappa} \ln (E y^+) + P \right]} \tag{16}$$

where the empirical P function is specified as:

$$P = \frac{\pi/4}{\sin (\pi/4)} \left(\frac{A}{\kappa} \right)^{1/2} \left(\frac{Pr}{Pr_t} - 1 \right) \left(\frac{Pr_t}{Pr} \right)^{1/4} \tag{17}$$

and the wall temperature T_w is a constant in the present work, $T_w = 2T_0$.

2.4. *Numerical procedure*

A numerical procedure, based on the SOLA algorithm [9], was modified by the authors' group for the investigation of the velocity and temperature fields in three-dimensional laminar channel flows with longitudinal vortex generators [3]. In the present work, this procedure has been extended to solve turbulent problems.

The SOLA algorithm solves the time dependent Navier–Stokes equations directly for the primitive variables by advancing the solution explicitly in time. The modification used here retains the solution route of the SOLA algorithm; an explicit time step for the momentum equations is followed by an implicit, iterative pressure and velocity upgrading. Since the flow field is uncoupled from the temperature field, they are determined in the following four steps:

(1) A new velocity field is determined for the new time step from the momentum equations with use of velocity, turbulence variables (k and ε) and pressure at the old time.
(2) The updated velocity field is corrected to obtain the pressure field at the new time step by an iterative procedure with aid of continuity equation until a divergence free velocity field is reached within a prescribed tolerance.
(3) The fields of turbulence variables are updated using their old time values and velocity field at the new time step.
(4) After convergence of the flow field calculation, the temperature field is determined by solving the energy equation iteratively with known velocity and turbulence fields.

The convergence criterion is the maximum gradient of the dependent variables $\max \{\Delta f/\Delta t\}$ in the whole domain, where Δf denotes the iteration difference of the dependent variables between two consecutive time levels and Δt denotes the advancing time step respectively. For a converged solution the $\max \{\Delta f/\Delta t\}$ should be less than 10^{-3}.

In order to validate the modified computer program, the code has been used to simulate the well documented three-dimensional turbulent flow experiments of Pauley and Eaton [4]. The comparison of the numerical and experimental results indicated a good agreement [10].

3. RESULTS AND DISCUSSION

Computations have been performed on a SUN 4/260 workstation. $91 \times 15 \times 48$ grid points and 60 CPU h have been used e.g. for the configuration in Fig. 4. The Reynolds number Re_H based on the channel height for all calculations is taken to be 50000 and the Prandtl number Pr is 0.7. For the sake of comparison, a hydrodynamically developed thermally developing turbulent channel flow (without vortex generator) is calculated with the same flow and

boundary conditions as described above. Henceforth this flow is referred to as the base flow.

Figure 5 shows typical computational results of cross stream velocity vectors at $x/H = 1.3$, 2.3, 4.3 and 9.3 in the channel with a pair of delta winglets. The generation and transport of the longitudinal vortices, eventual flattening of the vortex cores and their lateral movement towards the side boundaries are evident in this figure.

Figure 6 shows the temperature field for the same case as in Fig. 5. Isotherms in the base flow will be straight lines parallel to the upper and lower walls. In the flow with vortices, however, isotherms with large values appear around the vortex generator due to the high heat transfer there. At $x/H = 1.3$, the vortex cores are displayed by the variation of the isotherms 2 to 10. The empty white area corresponds to the isotherm 1 ($T/T_0 = 1$), i.e. the flow has not yet been heated up.

In successive cross sections ($x/H = 2.3$, 4.3 and 9.3) the mixing of hot and cold fluids due to azimuthal velocities of the vortices become evident and higher isotherms (lines 4 and 5) appear in the middle of the channel. The effect of the secondary flow on the temperature field is clear at the downstream location $x/H = 4.3$. In the upwash regions, i.e. in the area between the vortices near the upper wall and in the area of the outer region near the lower wall, the secondary flow is directed away from the wall and it sweeps the hot fluid to the core of the channel. In the downwash regions, i.e. in the area between the vortices near the lower wall and in the area above the vortex at the outer side, the strong downflow and lateral flow push the cold fluid from the core of the channel to the walls.

The dotted lines (isotherm 2) near the upper and lower walls at sections $x/H = 4.3$ and 9.3 show the extent of heating in the base flow. The thermal boundary layer in the channel is strongly disturbed by the longitudinal vortices.

Figure 7 shows the contour of the turbulent kinetic energy ratio k/k_0 for the above case, where k_0 is the k-value in the base flow. Higher turbulent kinetic energy is produced around the vortex generators by

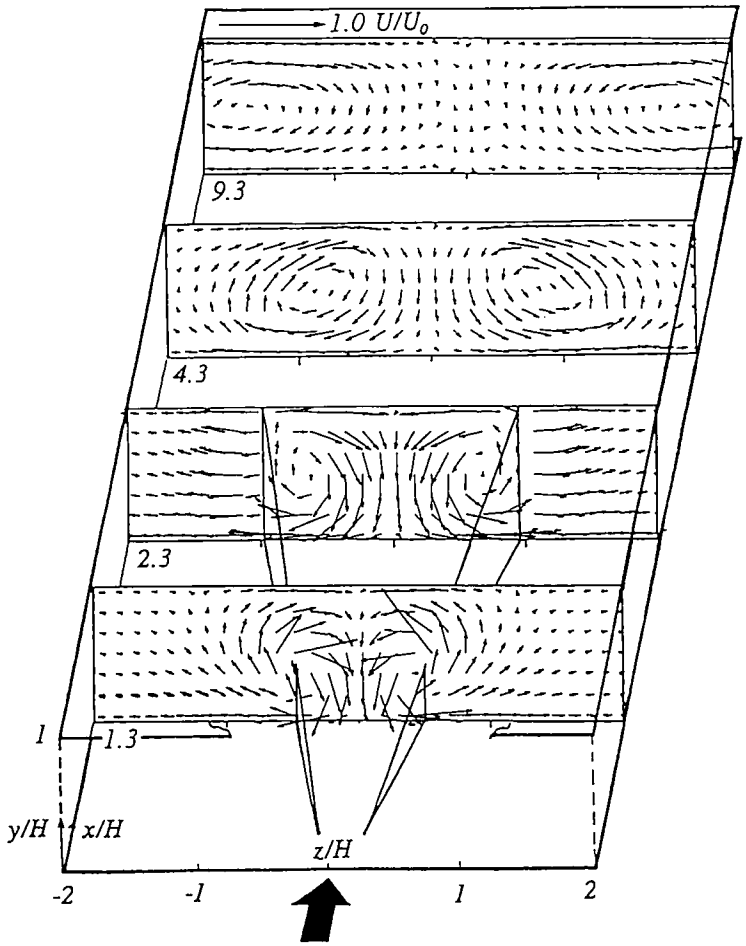

FIG. 5. Cross sectional velocity vectors at axial locations $x/H = 1.3$, 2.3, 4.3 and 9.3, showing the formation and development of longitudinal vortices in a channel with a delta winglet pair.

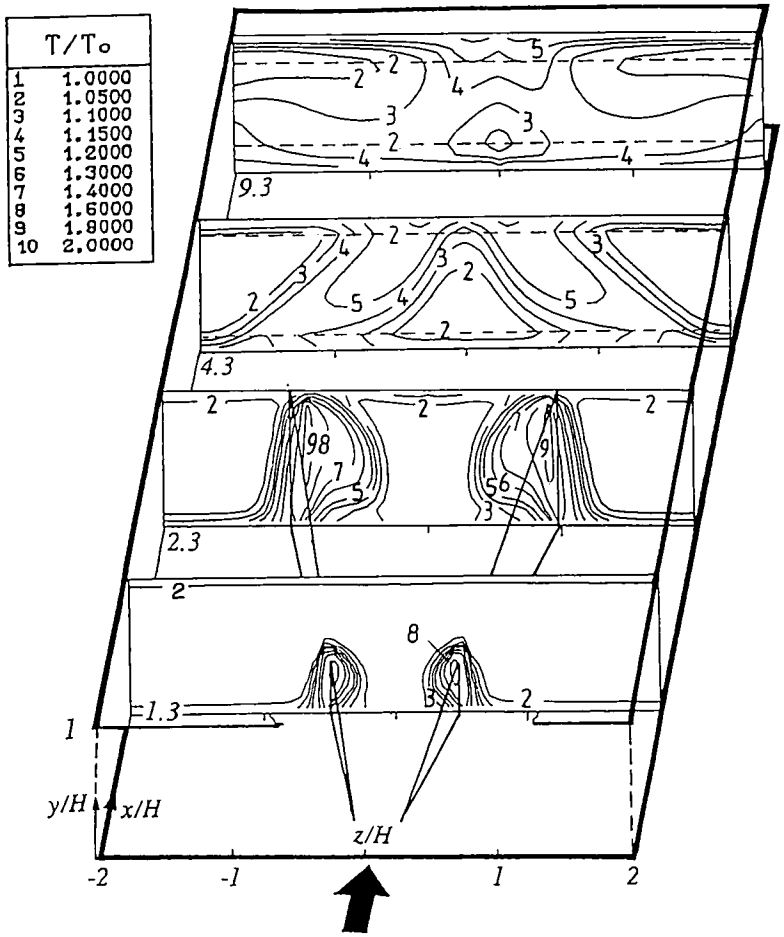

FIG. 6. Structure of the temperature field in a turbulent channel flow with a delta winglet pair: isotherms for a temperature ratio of $T_w/T_o = 2$ at cross sections $x/H = 1.3$, 2.3, 4.3 and 9.3; $Re_H = 50\,000$, $Pr = 0.7$.

the interaction between the main flow and the vortex generators. In the core region of the vortices at cross section $x/H = 2.3$ the turbulence energy is 100 times of that in base flow (line 9). At $x/H = 9.3$, k diffuses throughout the cross section in such a way that except in the upwash and downwash regions near the upper and lower walls (isoline 2) it is everywhere larger than that in the base flow. Large k signifies large turbulent thermal diffusivity and hence large heat transfer.

The flow and temperature fields with rectangular wing, delta wing and rectangular winglet pair will not be displayed further. In the following a comparison of the global characters of the flows with different vortex generators are presented.

Figure 8 compares the average vorticity component $\bar{\omega}_x$ in the channel with DWP, DW, RW and RWP. Here $\bar{\omega}_x$ is defined by:

$$\bar{\omega}_x = \frac{1}{A_f/2} \int_0^{A_f/2} |\omega_x| \, dA|_x ;$$

with

$$\omega_x = \frac{\partial W}{\partial y} - \frac{\partial V}{\partial z}. \tag{18}$$

All configurations show peaks in $\bar{\omega}_x$ distribution slightly in front of the trailing edge of the wing. The peak values for wings are 40–50% larger than for the corresponding winglets. However the decay in $\bar{\omega}_x$ for winglets is much slower than for wings. At the exit ($x/H = 10$), $\bar{\omega}_x$ for RWP is 70% larger than for RW. Since $\bar{\omega}_x$ can be used as a measure of the circulation, Fig. 8 also shows that the circulation in the channel with winglets has become nearly constant at $x/H = 4$ whereas with wings the circulation has not reached its constant value even at the exit.

Figure 9 compares the ratios of the spanwise averaged Nusselt numbers with (Nu_x) and without vortices (Nu_{ox}) in the channel for different vortex generator configurations. The Nusselt number is evaluated by:

$$Nu = \frac{Re\, Pr\, q_w}{c_p \rho U_o (T_w - T_B)}. \tag{19}$$

Equation (19) is derived from:

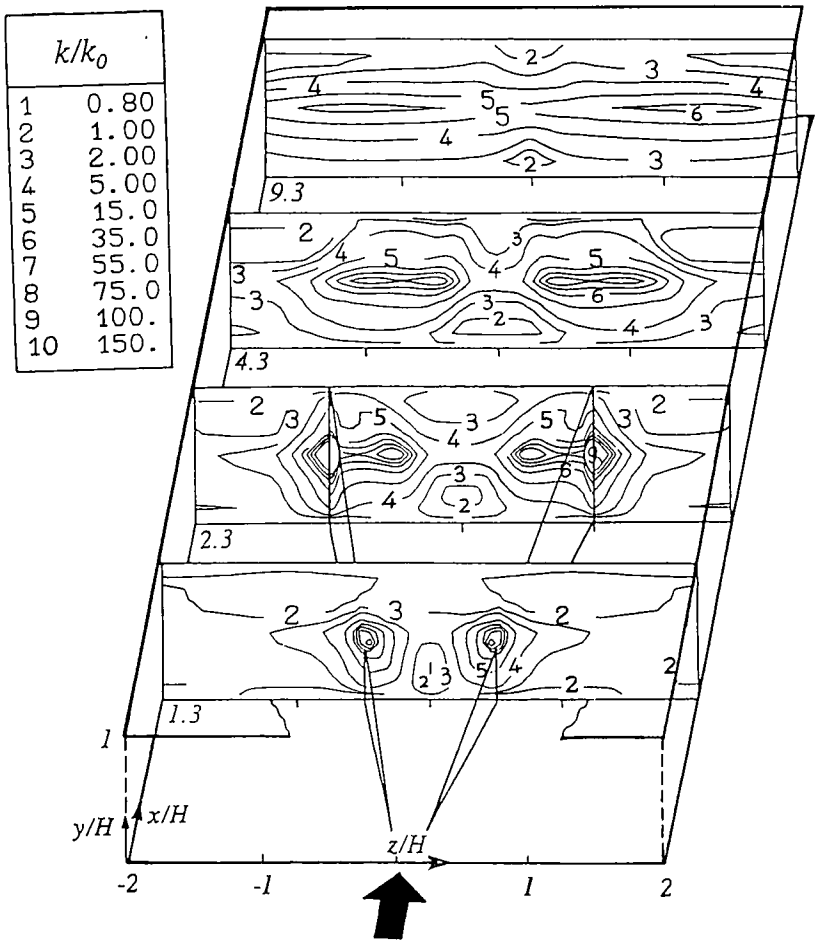

FIG. 7. Elevation of turbulent kinetic energy in the channel with a built-in delta winglet pair (Fig. 4), $Re_H = 50\,000$.

$$Nu = \frac{\alpha D_h}{\lambda} \tag{20}$$

with the aid of $q_w = \alpha (T_w - T_B)$ and the definitions of Re and Pr.

The spanwise averaged Nusselt number Nu_x is defined as:

$$Nu_x = \frac{1}{B}\int_{-B/2}^{B/2} Nu\, dz|_x. \tag{21}$$

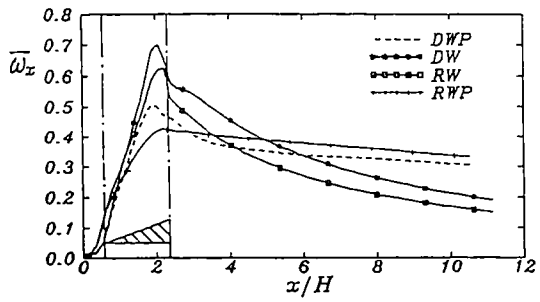

FIG. 8. Cross sectional averaged vorticity along the streamwise direction for the four vortex generators, showing strength and decay of longitudinal vortices.

The ratio Nu_x/Nu_{ox} indicates the streamwise heat transfer enhancement produced by the vortex generators. On the lower wall where the vortex generators are fixed, the Nu_x/Nu_{ox} distributions for the wings show a sharp change with peak and minimum near the base of the wing. These are caused by the spanwise flow acceleration at the pressure side due to the streamwise blockage and the flow separation at the suction side of the wing. Winglets whose span, unlike those of wings, are not normal to the main flow, do not generate sharp rise and fall in Nu_x. The Nu_x-enhancement due to vortices appears downstream of the vortex generators. For delta winglets, the flow does not separate at the suction side and further downstream the vortices enhance Nu_x. Hence, the smooth increase in Nu_x.

On the upper wall the rectangular wings cause the highest enhancement in Nu_x. This is probably because

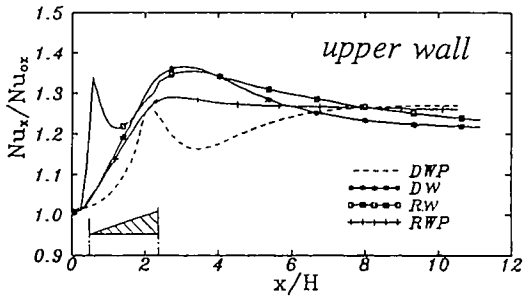

A)

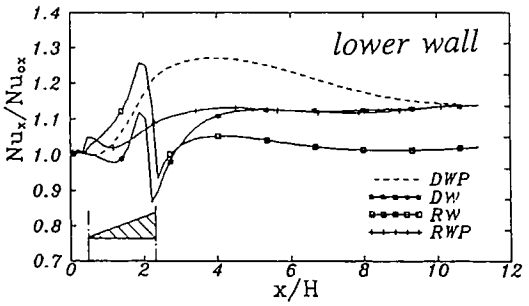

B)

FIG. 9. Ratios of the spanwise averaged Nusselt numbers on the A) upper and B) lower wall for flows with and without vortex generator, comparing the streamwise effects of the four vortex generators on heat transfer; $A_L/A_w = 30$, $\beta = 25°$, $Re_H = 50\,000$, $Pr = 0.7$.

the vortices generated by the rectangular winglets move closer to the upper wall.

The flow losses are evaluated by using the kinetic energy equation suggested by Gersten [11], which is simplified for the present problem as follows:

$$\Phi_{12} = \tfrac{1}{2}(\alpha_1 - \alpha_2)U_o^2 + \frac{p_1 - p_2}{\rho} \tag{22}$$

where

$$\Phi_{12} = \frac{P_D}{M} \tag{23}$$

is the specific dissipation. The variables α and P_D in equations (22) and (23) are kinetic energy correction factor and dissipation respectively, which are described in detail by Gersten in ref. [11]. The dissipation P_D indicates the loss of mechanical energy due to friction and turbulent mixing. For the convenience of analysis, a dimensionless number, called dissipation number [12], is derived from equation (22):

$$C_\varphi = \frac{\Phi_{12}}{U_o^2}\cdot\frac{H}{\Delta x} = \tfrac{1}{2}(\alpha_1 - \alpha_2)\frac{H}{\Delta x} + f_{app} \tag{24}$$

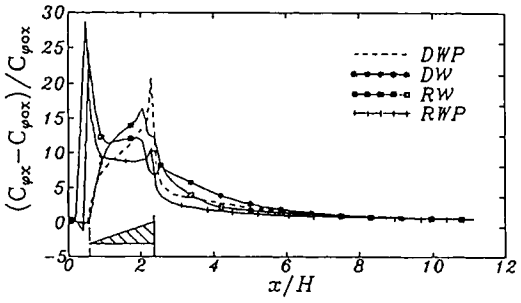

FIG. 10. Relative increase of the dissipation number C_φ, showing the additional flow losses caused by the vortex generators along streamwise direction; $Re_H = 50\,000$.

with the apparent friction factor f_{app} defined by Shah and London [13]

$$f_{app} = \frac{1}{2}\frac{p_1 - p_2}{(\rho/2)U_o^2}\frac{H}{\Delta x}. \tag{25}$$

In equation (24) the index 1 means inlet, index 2 means an arbitrary axial location at the downstream and Δx indicates the distance between the locations 1 and 2.

Figure 10 shows the relative increase of the dissipation numbers $(C_{\varphi x} - C_{\varphi o})/C_{\varphi o}$ over the base flow value $C_{\varphi o}$ for the four investigated cases. $C_{\varphi o}$ is independent of streamwise position in a hydrodynamically fully developed channel flow. The peak values of $(C_{\varphi x} - C_{\varphi o})/C_{\varphi o}$ appear at the leading edge for the rectangular wing and rectangular winglet pair whereas for the delta geometries the peaks appear near the trailing edge. From $x/H = 8$ downwards, the curves for all four vortex generator geometries merge together.

Table 2 compares the global increase of Nusselt numbers and flow losses for the four types of vortex generators relative to the base flow. The ratio of the channel wall to vortex generator areas A_L/A_w is 30 for all cases. The subscript m stands for the average value. It is interesting to see from the data in Table 2 that except for the delta winglet pair all vortex generators produce much more heat transfer enhancement at the upper wall than at the lower wall. The enhancement of Nusselt number averaged over both walls differs by only 3% for different types of vortex generators. The increase in flow losses for the four geometries can differ by more than 20%. For nearly equal heat transfer enhancement the rectangular winglet pair brings the least flow loss increase among the four vortex generators.

4. CONCLUSIONS

Heat transfer augmentation in turbulent flows in a channel with longitudinal vortex generators is caused by the elevation in the turbulent kinetic energy level near the wall and exchange of the fluid between the near wall and core region of the channel.

Table 2. Comparison of global effects of the four vortex generators on heat transfer and flow losses in turbulent channel flow; $T_w = 2T_0$, $A_L/A_w = 30$, $\beta = 25$, $R_H = 50\,000$, $Pr = 0.7$

	$Nu_m Nu_{om}$ upper wall	Nu_m/Nu_{om} lower wall	Nu_m/Nu_{om} average for both walls	$C_{\varphi m}/C_{\varphi o}$
DWP	1.20	1.18	1.19	4.2
RWP	1.24	1.10	1.17	4.0
DW	1.25	1.08	1.165	5.1
RW	1.28	1.04	1.16	4.9

$Nu_{om} = 230$; $C_{\varphi om} = 4.6 \times 10^{-3}$.

The mean heat transfer enhancement at an angle of attack of 25 and $Re_H = 50\,000$ amounts to 16–19% on a channel wall area which is 30 times larger than the face area of the vortex generator, the corresponding increase in flow losses is however 4–5 times larger than that in a turbulent channel flow without vortex generator.

The results in Table 2 indicate that the type of vortex generator should be chosen according to the application requirements, i.e. in the situation where the demands on heat transfer augmentation are equal for the two channel walls, delta winglet pairs should be the better choice; otherwise delta wing, rectangular wing or rectangular winglet pairs may be more suitable. In the latter case, the ratios of heat transfer enhancement to flow loss increase suggest better performance of the rectangular winglet pair than of other forms of vortex generators.

Acknowledgement—J. X. Zhu wishes to acknowledge gratefully the scholarship provided by German Aerospace Research Establishment (Deutsche Forschungsanstalt für Luft- und Raumfahrt).

REFERENCES

1. F. J. Edwards and C. J. R. Alker, The improvement of forced convection surface heat transfer using surface protrusions in the form of (A) cubes and (B) vortex generators, *Proc. 5th Int. Heat Transfer Conference*, Vol. 2, pp. 244–248 (1974).
2. M. Fiebig, P. Kallweit and N. K. Mitra, Wing type vortex generators for heat transfer enhancement, *Proc. 8th Int. Heat Transfer Conference*, Vol. 6, pp. 2909–2914 (1986).
3. M. Fiebig, U. Brockmeier, N. K. Mitra and Th. Güntermann, Structure of velocity and temperature fields in laminar channel flows with longitudinal vortex generators, *Numerical Heat Transfer, Part A* **15**, 281–302 (1989).
4. W. R. Pauley and J. K. Eaton, Experimental study of the development of longitudinal vortex pairs embedded in a turbulent boundary layer, *AIAA J.* **26**, 816–823 (1988).
5. T. Shizawa and J. K. Eaton, Interaction of an embedded longitudinal vortex with an attached three-dimensional turbulent boundary layer, Rept, MD-56, Thermosciences Division, Dept. Mech. Engr., Stanford University (1990).
6. J. O. Hinze, *Turbulence* (2nd Edn). McGraw-Hill, New York (1975).
7. B. E. Launder and D. B. Spalding, The numerical computation of turbulent flows, *Computer Methods in Applied Mechanics and Engineering* **3**, 269–289 (1974).
8. W. Rodi, *Turbulence Models and Their Application in Hydraulics*. Book Publication of International Association for Hydraulic Research, Delft, Netherlands (1980).
9. C. W. Hirt, B. D. Nichols and N. C. Romero, SOLA—A numerical solution algorithm for transient fluid flows, Los Alamos Scientific Laboratory Rept. LA-5652, Los Alamos, New Mexico (1975).
10. J. X. Zhu, M. Fiebig and N. K. Mitra, Numerical simulation of a 3-D turbulent flow field with longitudinal vortices, *ASME Special Publications*, FED-Vol. 103, pp. 131–136 (1990).
11. K. Gersten, Fluid mechanics and heat transfer; introduction and fundamentals. In *Heat Exchangers Design Handbook*, Vol. 2, chapter 2.2.1-4. Hemisphere, New York (1983).
12. U. Brockmeier, Numerisches Verfahren zur Berechnung dreidimensionaler Strömungs- und Temperaturfelder in Kanälen mit Längswirbeler-zeugern und Untersuchung von Wärmeübergang und Strömungsverlust, Dissertation, Ruhr-Universität Bochum, Germany, pp. 65, (1987).
13. R. K. Shah and A. L. London, Laminar flow in forced convection in ducts. In *Advances in Heat Transfer*. Academic Press, New York (1978).